

Role of shear induced diffusion in acoustophoretic focusing of dense suspensions

S. Karthick and A. K. Sen

Citation: *Appl. Phys. Lett.* **109**, 014101 (2016); doi: 10.1063/1.4955274

View online: <http://dx.doi.org/10.1063/1.4955274>

View Table of Contents: <http://aip.scitation.org/toc/apl/109/1>

Published by the [American Institute of Physics](#)



Small Conferences. BIG Ideas.

Applied Physics
Reviews

SAVE THE DATE!
3D Bioprinting: Physical and Chemical Processes
May 2–3, 2017 • Winston Salem, NC, USA

The banner features a background image of a blue, branching, 3D-printed structure resembling a biological vessel or network. The AIP Publishing HORIZONS logo is in the top left, and the event details are centered and right-aligned.

Role of shear induced diffusion in acoustophoretic focusing of dense suspensions

S. Karthick and A. K. Sen^{a)}

Department of Mechanical Engineering, Indian Institute of Technology Madras, Chennai-600036, India

(Received 6 May 2016; accepted 23 June 2016; published online 5 July 2016)

We investigate the interplay between acoustic and shear induced diffusion (SID) forces in acoustophoretic focusing of dense suspensions in a microchannel. A theoretical model is presented which accurately predicts the width of the focused band in terms of shear rate, acoustic energy density, and particle concentration. The role of SID is clearly demonstrated by switching off the acoustic field, which leads to the instantaneous spreading of the focused band. At a given acoustic energy density and particle concentration, there exists a critical shear rate Γ_{cr} above which the focusing of microparticles is prevented. For $\Gamma < \Gamma_{cr}$, an equilibrium focused band is formed whose width remains constant downstream. *Published by AIP Publishing.*

[<http://dx.doi.org/10.1063/1.4955274>]

The physics of migration of microparticles in a flow of dilute suspensions (negligible particle-particle interactions) subjected to acoustic standing wave inside a microchannel is well established.^{1,2} In acoustophoresis, there are two forces mainly responsible for particle migration: primary radiation force and secondary radiation force. Secondary forces on particles in a dilute suspension are negligible due to less interaction between particles; thus, the balance between drag and primary acoustic radiation forces determines particle trajectories.² The particles in dilute suspensions migrate towards either node if contrast factor is positive or antinode if contrast factor is negative, irrespective of the acoustic energy density.³ Acoustophoretic (ACP) focusing of microparticles in dense suspensions finds many important applications, including blood plasma separation.⁴ However, the underlying physics of acoustophoretic migration of microparticles in a flow of dense suspensions subjected to acoustic standing wave is not studied so far.⁴ Moreover, there has been a general misconception that if adequate acoustophoretic force and time or channel length is provided, the microparticles would eventually be focused to a narrow band to enable separation.⁴ Unlike dilute suspensions, in a flow of highly concentrated suspensions, we show that the shear induced diffusion (SID) plays a major role in the migration of microparticles. We show that the competition between acoustic radiation force and SID is critical in determining the width of the focused band. The prediction of the width of focused band and consequently the width of the particle-free region has great relevance in the acoustophoretic separation of plasma from whole blood. SID is the diffusive motion of microparticles in a shear flow due to the hydrodynamic interactions between the neighbouring particles.⁵⁻⁷ In SID, the cross stream-wise distance between neighbouring particles after interaction increases as compared to that before interaction.⁸ Here, we analyse the interplay between acoustic and SID forces to explain the physics of acoustophoretic

migration of microparticles (RBCs) in dense suspensions (blood) in a microchannel.

The primary acoustic radiation force acting on a small spherical particle of radius smaller than acoustic wavelength (i.e., $a \ll \lambda$) is governed by^{1,2}

$$F_{ACP} = 4\pi a^3 E_{ac} k \sin(2kz) \varphi, \quad (1)$$

$$\varphi = \frac{\rho_p + \frac{2}{3}(\rho_p - \rho_o)}{2\rho_p + \rho_o} - \frac{1}{3} \frac{\rho_o c_o^2}{\rho_p c_p^2},$$

where F_{ACP} is the acoustophoretic radiation force, a is the radius of particle, E_{ac} is the acoustic energy density, k is the wave number, z is the distance from wall, φ is the contrast factor, ρ_p is the density of particle, ρ_o is the density of medium, c_p is the velocity of sound in particle, and c_o is the velocity of sound in medium. A microchannel of dimension of $180 \mu\text{m}$ (height) \times $400 \mu\text{m}$ (width) \times 40mm (length) is etched (Deep Reactive Ion Etching) in a silicon wafer (0.5 mm thick) and then sealed with a glass slide (0.5 mm thick) by anodic bonding. The acoustic energy density inside microchannel is proportional to voltage applied to PZT transducer (Sparkler Ceramics, India), which is bonded to a silicon-glass chip. Acoustic energy density inside microchannel for different applied voltages was measured by tracking polystyrene beads suspended in aqueous solution. The positions of particles were tracked frame by frame from video captured using a CCD camera (Dino-lite). By equating acoustic radiation force to drag the force acting on particles, an equation for velocity of particles at different positions is obtained. Upon integration of velocity, the equation for particle position is given by²

$$z(t) = \frac{1}{k} \arctan \left\{ \tan[kz(0)] \times \exp \left[\frac{4\varphi}{3} (ka)^2 \frac{E_{ac}}{\eta_f} t \right] \right\}. \quad (2)$$

In the above equation, on substituting the position of polystyrene particles at different times $z(t)$ obtained from experiments, the properties of the polystyrene beads, and the properties of aqueous solution, the values of E_{ac} at 5.0 V and 7.5 V were found to be 20.1 J/m^3 and 40.6 J/m^3 , respectively. Since Eq. (2) is only valid for spherical microparticles, in

^{a)} Author to whom correspondence should be addressed. Electronic mail: ashis@iitm.ac.in

order to obtain the acoustic energy density E_{ac} inside the microchannel, we have used spherical polystyrene microbeads instead of RBCs. The properties of polystyrene beads used to determine the acoustic energy density and properties of red blood cells used in our theoretical modeling and analysis are provided in the [supplementary material](#). The description and estimation of secondary radiation force acting on microparticles (RBCs) is presented and discussed in the [supplementary material](#). We show that acoustic secondary radiation force acting on RBCs is negligible compared to primary radiation force.

The diffusive flux due to SID in shear and vorticity directions in a simple shear flow can be expressed as $J_s = D^s \nabla \phi$ and $J_v = D^v \nabla \phi$, where D^s and D^v are the diffusivities in shear and vorticity directions, respectively.⁷ The diffusivities in shear and vorticity directions can be written as $D_s = D_s^* \dot{\gamma} a^2 f(\phi)$ and $D_v = D_v^* \dot{\gamma} a^2 f(\phi)$, where D_v^* is the dimensionless diffusivity in the vorticity direction, D_s^* is the dimensionless diffusivity in the shear direction, $\dot{\gamma}$ is the local shear rate, a is the radius of particle, $f(\phi) = \phi$, if the concentration is low (volume fraction $\phi < 0.1$, dilute suspension). For high concentrations ($\phi > 0.1$, dense suspensions), various closures for $f(\phi)$ have been proposed.^{5,9-11} Here, we use the recently published closure based on microfiltration¹¹

$$f(\phi) = 1.5 (1 - \phi)^2 (\tilde{\phi} / \phi_{max}) \{1 + \tilde{\phi} / (1 - \tilde{\phi})\}, \quad (3)$$

where $\tilde{\phi} = \phi / \phi_{max}$, ϕ_{max} is the random closed packing volume fraction of particles. For hard spheres, the value of ϕ_{max} is approximately 0.64, and for cut spheres having same aspect ratio as RBCs, ϕ_{max} is 0.765.¹² From Eq. (3), it is important to note that the shear induced diffusion flux diverges when the local concentration of the suspension ϕ approaches random closed packing volume fraction ϕ_{max} . The dimensionless diffusivities of RBCs, which are deformable,¹³ in shear (D_s^*) and vorticity (D_v^*) directions, are reported as 1.77 and 0.12, whereas for hard spheres, D_s^* and D_v^* are 0.2 and 0.03.¹⁴ The Reynolds number in our study is in the range of 0.04 to 4. Thus, the inertial lift force can be neglected, but the non-inertial lift force of RBCs in shear flow near the wall would create a cell free layer. However, at high hematocrit concentrations, the cell free layer thickness is only $\sim 1 \mu\text{m}$,¹⁵ so we neglect the effect of the non-inertial lift force when compared to that of SID. The particle-particle interactions¹⁶ due to van der Waals force which may be responsible for the aggregation of RBCs is neglected in our model because of much higher shear rate used in the present study. From

experiments and theory, it has been shown that the aggregation of RBCs is observed only if the suspension is at rest or flowing at lower shear rates ($\sim 10 \text{ s}^{-1}$) and for shear rates above 60 s^{-1} , aggregation is not observed.¹⁷

In our study, for convenience, we consider particles whose contrast factor is positive in fluid medium so that these particles migrate to the center (node) of the channel under acoustic standing wave. When suspension enters the microchannel subjected to acoustic standing wave, microparticles tend to migrate toward the center of the channel which in turn creates a particle-free fluid layer near the wall. A nonhomogeneous concentration profile is created across the microchannel along the acoustic standing wave direction. The migration of particles due to acoustophoretic force is opposed by SID force due to the non-zero concentration gradient and shear rate. The concentration profile evolves along the length of the channel due to the imbalance between the acoustic radiation and SID forces acting on the microparticles. After some distance or time, acoustic radiation force is balanced by SID, thereby establishing an equilibrium RBC band as shown in Fig. 1(a). The experimental images showing evolution of the RBC band at different locations along the length of the channel are shown in Fig. 2. The dependence of width of the focused RBC band w_{cx} with the shear rate and concentration is depicted in Fig. 3. The results clearly show that for $x > x_c$, the equilibrium width of the focused RBC band w_c remains unchanged downstream due to the SID force acting on the RBCs, which prevents further focusing of the RBCs. The location at which the equilibrium width is achieved was found to be a function of the shear rate, concentration, and energy density, i.e., $x_c = f(\dot{\gamma}, E_{ac}, \phi)$. The magnitude and directions of diffusive fluxes due to SID and ACP shortly after the suspension enters into the acoustic zone of microchannel are depicted in Fig. 1(b), whose relevance is explained later.

The presence of SID force is clearly demonstrated by the evolution of the focused RBC stream after switching off the acoustic field, as shown in Fig. 4. At $10 \mu\text{l}/\text{min}$ ($\Gamma = 67.331/\text{s}$), the average velocity in the microchannel is $2.3 \text{ mm}/\text{s}$. Upon switching off the acoustic field, it takes 1.8 s for the RBCs to redistribute and spread throughout the channel cross-section. The time required for the unfocused RBCs to reach downstream ($x = 4.0 \text{ cm}$) from upstream ($x = 1.0 \text{ cm}$) is approximately 13.0 s , which is one order of magnitude higher compared to the redistribution time (1.8 s). Thus, it is confirmed that diffusion of the band of focused microparticles on switching off the acoustic field is due to SID and not because of the unfocused cells coming

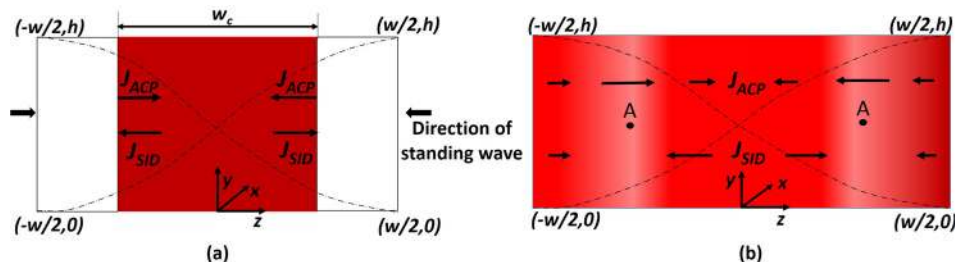


FIG. 1. (a) The schematic of the cross-section of a rectangular microchannel showing the focused RBC band, acoustic standing wave with nodes and antinodes, and directions of diffusive fluxes due to acoustic radiation force and SID. (b) The magnitude and directions (arrows) of diffusive fluxes due to SID and ACP shortly after the suspension enters into the acoustic zone of microchannel, acoustic force is maximum at region A.

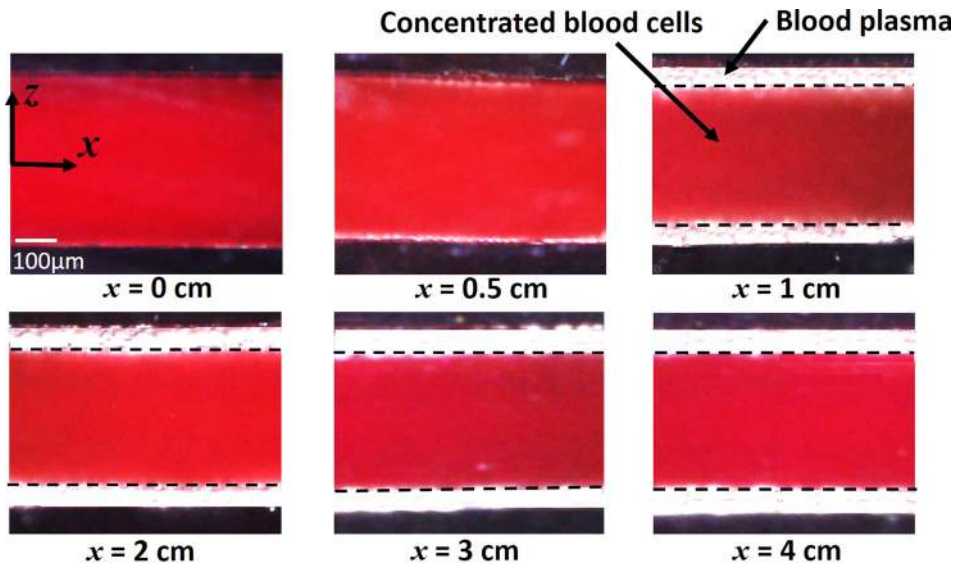


FIG. 2. The evolution of the width of the focused RBC band at different positions along the length of the microchannel, whole blood (42.5% hematocrit), flow rate of $10 \mu\text{l}/\text{min}$ ($\Gamma = 67.33 \text{ 1/s}$), and acoustic energy density of 40.6 J/m^3 .

from upstream. Table I shows a comparison of the time required to undo the effect of acoustophoretic focusing with that for the initial focusing of particles in the beginning when acoustic field is turned on, at different energy densities and shear rates. The time taken for the redistribution of RBCs is smaller as compared to that for the initial focusing because when acoustic field is turned on, acoustic force competes with the SID for the focusing to take place but when it is turned off only SID force exists which quickly diffuses particles to their initial distribution.

The steady advection diffusion equation can be written as

$$u(y, z) \frac{\partial \phi}{\partial x} = -\frac{\partial J_y}{\partial y} - \frac{\partial J_z}{\partial z}, \quad (4)$$

where J_z and J_y are diffusive fluxes in the z and y directions, respectively. Here, $J_z = J_{SID,z} + J_{ACP,z}$ and $J_y = J_{SID,y}$, where J_{SID} and J_{ACP} are diffusive fluxes due to primary acoustic radiation force and shear induced diffusion. Since primary acoustic radiation force acting in the y -direction is zero, we can assume that the concentration in the y -direction is homogenous, $\partial \phi / \partial y = 0$ and $J_y = J_{SID,y} = 0$. The diffusive flux in the z -direction can be written as¹⁴

$$J_{SID,z} = -a^2 f(\phi) \frac{\partial \phi}{\partial z} \frac{[D_v^* \dot{\gamma}_y^2 + D_s^* \dot{\gamma}_z^2]}{\sqrt{\dot{\gamma}_y^2 + \dot{\gamma}_z^2}}. \quad (5)$$

The diffusive flux due to acoustophoresis can be written as $J_{ACP,z} = (F_{ACP} \phi / 6\pi \eta_{eff} a)$, where η_{eff} is the effective viscosity of the suspension, which is $\eta_{eff} = \eta_f / (1 - \phi)^2$.¹⁶ Thus, Eq. (4) reduces to

$$u(y, z) \frac{\partial \phi}{\partial x} = -\frac{\partial}{\partial z} \left[-\frac{a^2 f(\phi)}{\sqrt{\dot{\gamma}_y^2 + \dot{\gamma}_z^2}} \frac{\partial \phi}{\partial z} [D_v^* \dot{\gamma}_y^2 + D_s^* \dot{\gamma}_z^2] + \frac{F_{AC}}{6\pi \eta_{eff} a} \phi \right]. \quad (6)$$

When the highly concentrated suspension enters into the acoustic field, the evolution of the concentration profile is determined by Eq. (6). At some location (after some time) downstream, the steady concentration profile $J_z = 0$ is established due to the balance between the acoustic radiation force and shear induced diffusion. So, Eq. (6) reduces to

$$\frac{a^2 f(\phi)}{\sqrt{\dot{\gamma}_y^2 + \dot{\gamma}_z^2}} \frac{\partial \phi}{\partial z} [D_v^* \dot{\gamma}_y^2 + D_s^* \dot{\gamma}_z^2] = \frac{F_{AC}}{6\pi \eta_{eff} a} \phi. \quad (7)$$

F_{ACP} acting on RBCs is strongly dependent upon the orientation of RBCs with respect to the acoustic field. The shear rate is a function of both the y - and z -directions. Thus, an analytical solution of the Eq. (7) is beyond the scope of the present work, and we proceed with scaling analysis. We scale $\partial \phi / \partial z \sim \phi / w_c$, $\dot{\gamma}_y \sim \langle \dot{\gamma}_{y=h} \rangle_z$, $\dot{\gamma}_z \sim \langle \dot{\gamma}_{z=w/2} \rangle_y$, and $\sin(2kz) \sim 1$, where w_c is the width of the focused band of RBCs, $\langle \dot{\gamma}_{y=h} \rangle_z$ is the average shear on the top surface, and $\langle \dot{\gamma}_{z=w/2} \rangle_y$ is the average shear on the sidewall. So, Eq. (7) is reduced to

$$\frac{f(\phi)}{w_c} \left[\frac{D_v^* \langle \dot{\gamma}_{y=h} \rangle_z^2 + D_s^* \langle \dot{\gamma}_{z=w/2} \rangle_y^2}{\sqrt{\langle \dot{\gamma}_{y=h} \rangle_z^2 + \langle \dot{\gamma}_{z=w/2} \rangle_y^2}} \right] = C \frac{2E_{ac} k \phi}{3\eta_{eff}}. \quad (8)$$

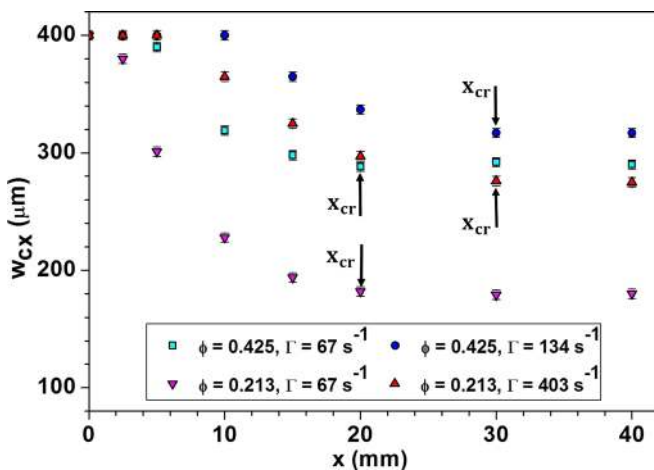


FIG. 3. The evolution of the width of the focused RBC band at different positions along the length of the microchannel, concentrations, and shear rate, $E_{ac} = 40.6 \text{ J/m}^3$.

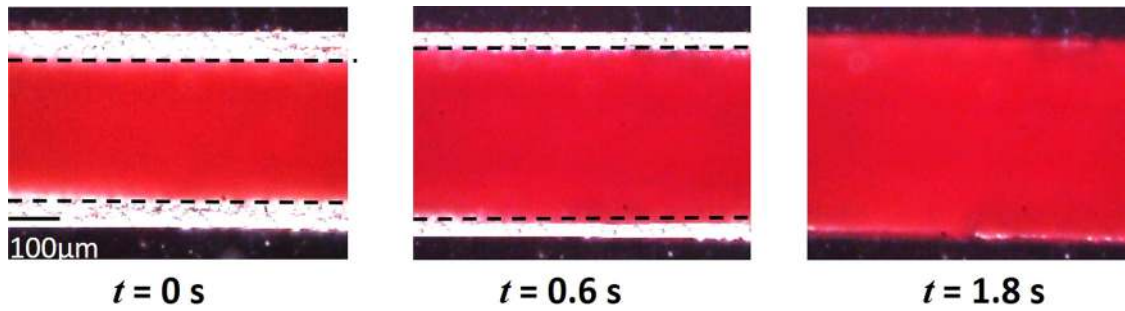


FIG. 4. The evolution of the width of the focused RBC band at $x = 4$ cm immediately after switching off the acoustic field (i.e., $E_{ac} = 0$ at $t = 0$, focused band at $t < 0$ with 40.6 J/m^3), flow rate of $10 \text{ } \mu\text{l/min}$ ($\Gamma = 67.33 \text{ 1/s}$), unfocusing of RBCs due to SID is observed.

TABLE I. Focusing and unfocusing time for cells (42.5% hematocrit) at different energy densities and shear functions.

S. No.	Energy density E_{ac} (J/m^3)	Shear function Γ (1/s)	Initial width w (μm)	Focused width w_c (μm)	Focusing time (s) (SID vs. ACP)	Unfocusing time (s) (Only SID)
1	20.1	33.63	400 ± 4	290 ± 4	$12.2 \pm .07$	$3.4 \pm .07$
2	40.6	33.63	400 ± 4	270 ± 4	$7.07 \pm .07$	$2.7 \pm .07$
3	20.1	67.33	400 ± 4	315 ± 4	$16.1 \pm .07$	$1.6 \pm .07$
4	40.6	67.33	400 ± 4	289 ± 4	$10.3 \pm .07$	$1.8 \pm .07$
5	40.6	134.66	400 ± 4	316 ± 4	$11.6 \pm .07$	$1.2 \pm .07$

For convenience, we define the shear rate function $\Gamma = (D_v^* \langle \dot{\gamma}_{y=h} \rangle_z^2 + D_s^* \langle \dot{\gamma}_{z=w/2} \rangle_y^2) / \sqrt{\langle \dot{\gamma}_{y=h} \rangle_z^2 + \langle \dot{\gamma}_{z=w/2} \rangle_y^2}$, so Eq. (8) gives

$$\frac{f(\phi)\Gamma}{w_c} = \frac{2C}{3} \left[\frac{kE_{ac}\phi}{\eta_{eff}} \right], \quad (9)$$

where C is the scaling constant. Here, $\langle \dot{\gamma}_{y=h} \rangle_z$ and $\langle \dot{\gamma}_{z=w/2} \rangle_y$ are calculated from velocity field for rectangular channel.¹⁷ The relationship between the two unknowns, cell fraction ϕ and width of band w_c , is obtained from mass balance $w_c \times \phi = w \times \phi_{in}$, where ϕ_{in} is the initial homogenous concentration of suspension. Eq. (9) becomes an implicit equation and only function of w_c , which is solved numerically using Newton-Raphson method. For all cases, the theoretical model is compared with the experimental data and was found to match well for the scaling constant $C = 0.18$ and $\phi_{max} = 0.8$. For RBCs, $\phi_{max} = 0.8$ is slightly higher than that of $\phi_{max} = 0.765$ for hard cut-spheres of the same aspect ratio, which might be due to the deformability of RBCs.

Experiments are carried out with dense suspensions using whole blood (42.5% hematocrit) and 1:1 diluted blood (21.25% hematocrit) samples, at various flow rates from 5 to $100 \text{ } \mu\text{l/min}$ with acoustic energy densities of 20.1 and 40.6 J/m^3 . The equilibrium width of the focused RBC band w_c is measured at the end of the microchannel at $x = 4$ cm. The variation in w_c with shear rate function Γ (controlled by varying flow rate Q , Γ linearly proportional to Q) at different concentrations ($\phi_{in} = 0.425$ and 0.213) and acoustic energy density E_{ac} , measured from experiments and predicted by the model, is depicted in Fig. 5. The model predictions are in good agreement with experimental data within a maximum error of 15%. The uncertainty in the measurement of the width of the focused band is $\pm 4 \text{ } \mu\text{m}$. As observed, the equilibrium width of the RBC band w_c increases with increase in the shear rate function (i.e., at higher Q). This can be directly

explained from Eq. (9) that at a fixed ϕ_{in} and E_{ac} , w_c has to increase to maintain a balance between the acoustic and SID forces at equilibrium. Similarly, it is observed that at a fixed ϕ_{in} and Γ , a higher E_{ac} leads to a smaller w_c , and at a fixed Γ and E_{ac} , a higher concentration of microparticles gives rise to a higher w_c . The above explanation holds true only when the shear rate function is below a critical Γ_{cr} . When $\Gamma \geq \Gamma_{cr}$, the RBCs completely spread across the channel cross-section, i.e., $w_c = w$ and the formation of particle-free layer is prevented. It is observed that Γ_{cr} is smaller at a lower E_{ac} and higher ϕ_{in} . It is interesting to note from Eq. (9) that the focused width is independent of the size of the RBCs but depends on the local volume fraction via $f(\phi)$. In a limiting case, when $\Gamma \rightarrow 0$, the volume fraction calculated using the focused band of RBCs shown in Fig. 5, at different initial

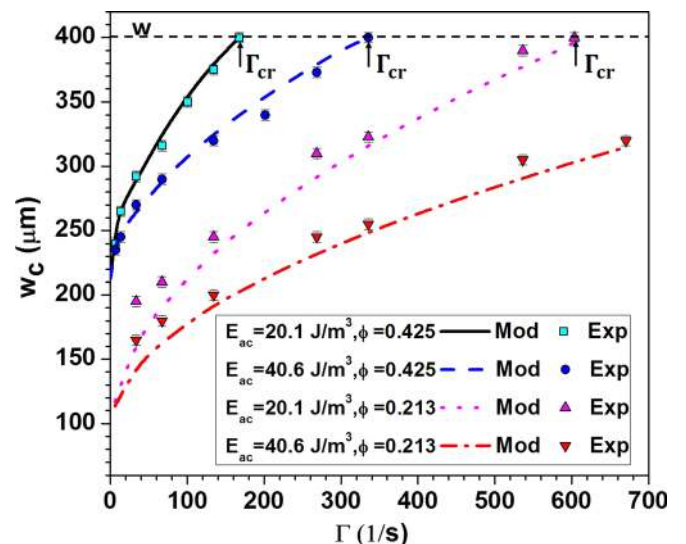


FIG. 5. Width of the focused width of the RBC band vs. shear rate function at different acoustic energy densities E_{ac} and initial volume fraction ϕ_{in} , channel width $w = 400 \text{ } \mu\text{m}$, when $w_c = w$ then $\Gamma = \Gamma_{cr}$.

concentration and E_{ac} come out to be 0.8, which is the random closed packing volume fraction ϕ_{max} .

From Fig. 3, it is observed that the shear rate function does not have a much impact on the channel length required for the focused stream to attain the equilibrium band which is counter intuitive because SID is directly proportional to the shear rate function. The results show that when the shear rate function is increased by 6-times (from $\Gamma = 67$ to 403 1/s), the channel length required for attaining the equilibrium band increases only 1.5 times (x_c from 20mm to 30mm). This behavior is explained as follows: there is a spatial variation of acoustic force across the microchannel width which is zero at the walls and center of the microchannel and maximum at the midpoint between the wall and center [2] (region A in Fig. 1(b)). As shown in Fig. 1(b), when a dense suspension just enters the acoustic zone, the microparticles at region A would move towards center faster than those located near to the walls; thus, in the beginning, the concentration of particles is more at the wall when compared with that at region A. So, at the beginning of the microchannel in the acoustic zone, SID enables particles to move towards region A from the wall, and the initial focusing of the microparticles is enhanced at higher shear rates. However, in the later part of the microchannel in the acoustic zone, the concentration of microparticles at the center increases significantly, and the SID force opposes the focusing of the microparticles further as discussed earlier.

In summary, we studied the role of shear induced diffusion (SID) in acoustophoretic focusing of microparticles in dense suspensions, which was not explained so far. Our results show the existence of an equilibrium focused RBC band, which clearly demonstrates the presence of SID that prevents particles from getting focused to any further to a narrower band. Moreover, SID causes almost instantaneous diffusion of particles in a focused band to its initial distribution as soon as the field is turned off. For a given initial concentration and acoustic energy density, there exists a critical value of the shear rate function above which the focusing of particles is prevented due to much stronger SID when compared to the acoustic force. In addition to acoustic energy

density, the local volume fraction and the shear rate function play a critical role in the focusing of microparticles in dense suspension. The model and results can be extremely important for many applications relating to the manipulation of microparticles under acoustic fields, for instance, in designing microfluidic systems to enhance separation of blood plasma from whole blood.

See [supplementary material](#) for the estimation and comparison of secondary radiation force with primary radiation force.

The authors would like to thank DST and DBT, India, and IIT Madras for providing the financial support for the project. They acknowledge MEMS Lab of EE, IIT Madras for supporting the fabrication work.

¹K. Yosioka and Y. Kawasima, *Acoustica* **5**, 167 (1955).

²H. Bruus, *Lab Chip* **12**, 1014 (2012).

³A. Lenshof, M. Evander, T. Laurell, and J. Nilsson, *Lab Chip* **12**, 684 (2012).

⁴A. Lenshof, A. Ahmad-Tajudin, K. Järås, A. M. Swärd-Nilsson, L. Åberg, G. Marko-Varga, J. Malm, H. Lilja, and T. Laurell, *Anal. Chem.* **81**, 6030 (2009).

⁵L. David and A. Acrivos, *J. Fluid Mech.* **181**, 415 (1987).

⁶F. R. da Cunha and E. J. Hinch, *J. Fluid Mech.* **309**, 211 (1996).

⁷R. Rusconi and H. A. Stone, *Phys. Rev. Lett.* **101**, 254502 (2008).

⁸T. Podgorski, N. Callens, C. Minetti, G. Coupier, F. Dubois, and C. Misbah, *Microgravity Sci. Technol.* **23**, 263 (2011).

⁹J. F. Morris and F. Boulay, *J. Rheol.* **43**, 1213 (1999).

¹⁰R. J. Phillips, R. C. Armstrong, R. A. Brown, A. L. Graham, and J. R. Abbott, *Phys. Fluids* **30**, 30 (1992).

¹¹H. M. Vollebregt, R. G. M. Van Der Sman, and R. M. Boom, *Soft Matter* **6**, 6052 (2010).

¹²A. Wouterse, S. R. Williams, and A. P. Philipse, *J. Phys. Condens. Matter* **19**, 406215 (2007).

¹³J. Kim, H. Lee, and S. Shin, *J. Cell. Biotechnol.* **1**, 63 (2015).

¹⁴X. Grandchamp, G. Coupier, A. Srivastav, C. Minetti, and T. Podgorski, *Phys. Rev. Lett.* **110**, 108101 (2013).

¹⁵T. Wang, U. Rongin, and Z. Xing, *Sci. Rep.* **6**, 20262 (2016).

¹⁶J. F. Brady, *J. Chem. Phys.* **99**, 567 (1993).

¹⁷H. Bruus, *Theoretical Microfluidics* (Oxford University Press, New York, 2008).